Chinese Journal of Aeronautics, (2015), 28(3): 946–953

Chinese Society of Aeronautics and Astronautics
& Beihang University

Chinese Journal of Aeronautics

cja@buaa.edu.cn
www.sciencedirect.com

Determination of optimal samples for robot calibration based on error similarity

Tian Wei *, **Mei Dongqi, Li Pengcheng, Zeng Yuanfan, Hong Peng, Zhou Wei**

College of Mechanical and Electronical Engineering, Nanjing University of Aeronautics and Astronautics, Nanjing 210016, China

Received 20 September 2014; revised 1 December 2014; accepted 19 January 2015
Available online 2 April 2015

KEYWORDS

Aircraft assembly;
Error compensation;
Positioning accuracy;
Robotics;
Sampling grid

Abstract Industrial robots are used for automatic drilling and riveting. The absolute position accuracy of an industrial robot is one of the key performance indexes in aircraft assembly, and can be improved through error compensation to meet aircraft assembly requirements. The achievable accuracy and the difficulty of accuracy compensation implementation are closely related to the choice of sampling points. Therefore, based on the error similarity error compensation method, a method for choosing sampling points on a uniform grid is proposed. A simulation is conducted to analyze the influence of the sample point locations on error compensation. In addition, the grid steps of the sampling points are optimized using a statistical analysis method. The method is used to generate grids and optimize the grid steps of a Kuka KR-210 robot. The experimental results show that the method for planning sampling data can be used to effectively optimize the sampling grid. After error compensation, the position accuracy of the robot meets the position accuracy requirements.

1. Introduction

The performance requirements for the new-generation aircraft assembly are higher than ever before. With high productivity, great flexibility, and low cost, articulated arm robots are used to improve assembly quality and production efficiency. Automatic drilling and riveting systems based on robots have been gradually implemented in Airbus and Boeing aircraft manufacturing systems.[1–5] Aircraft assembly requires equipment to have good absolute position accuracy (less than 0.5 mm). Therefore, it is necessary to improve the absolute position accuracy of industrial robots.

For ease of implementation and cost, the calibration method is more practical. Roth et al.[6] summarizes that robot calibration is an integrated process of modeling, measurement, identification, and implementation of a new model. One of the most difficult problems in robot calibration is choosing measurement samples to minimize the absolute position error based on an established error model. In fact, the sampling point locations have a great impact on the robot error compensation effect. Therefore, it is important to logically choose sampling points.

* Corresponding author. Tel.: +86 25 84891836.
E-mail address: tw_nj@nuaa.edu.cn (W. Tian).

Peer review under responsibility of Editorial Committee of CJA.

http://dx.doi.org/10.1016/j.cja.2015.03.003

There are many methods for robot calibration. In order to eliminate the singularity problem in the traditional D-H model proposed by Stone and Sanderson[7], several modeling methods including the S-model[8], the CPC (complete and parametrically continuous) kinematic model[9], and the modified D-H model[10] have been developed and used widely. A POE (product of exponentials) formula was used to calibrate serial robots[11], with which the singularity avoidance of the POE-based model was proved. A laser tracker was used for measurement and the robot parameter errors were identified.[12] A feasible low-cost vision-based measurement system using a single camera was developed for robot calibration methods and systems.[13] The Levenberg–Marquardt algorithm was used to identify the 25 unknown parameter errors described by the MD-H model.[14] Neural networks were also used to improve the poisoning accuracy of robot manipulators.[15] Park et al.[16] employed a stationary camera and a structured laser module (SLM) attached on a robot's end effector to measure the accurate position of the robot.[16] Several observability indexes were promoted to measure the goodness of a pose set based on analyzing the effects of noise and variance of parameters.[17]

From existing literature, most research focuses on model optimization, development of measuring equipment, and identification methods. Some methods use observability to judge the effectiveness of sampling points but not planning. In this study, a method is proposed for planning sampling points based on the error similarity compensation method.[18,19] In this method, sampling points are optimized while the accuracy is ensured. The number of sampling points is reduced to improve the implementation efficiency.

2. Error compensation method based on error similarity

2.1. Analysis of kinematics model error

The transformation matrix $\boldsymbol{T}_n$ that relates the tool frame {T} to the robot's base frame {B} can be represented as:

$$\boldsymbol{T}_n = \boldsymbol{A}_1\boldsymbol{A}_2\boldsymbol{A}_3\ldots\boldsymbol{A}_n \tag{1}$$

$$\boldsymbol{A}_i = \mathrm{Rot}(Z,\theta_i)\cdot\mathrm{Trans}(0,0,d_i)\cdot\mathrm{Trans}(a_i,0,0)\cdot\mathrm{Rot}(X,\alpha_i) \tag{2}$$

where $\boldsymbol{A}_i$ is the coordinate transformation matrix between joint $i-1$ and joint i, a_i is the length of the connecting rod of the ith joint, α_i is the torsional angle of the connecting rod of the ith joint, d_i is the joint deviation of the ith joint, and θ_i is the joint rotation angle of the ith joint, X is the X-axis of the link frame, Z is the Z-axis of the link frame.

According to Eq. (2), the description of $\boldsymbol{A}_i$ depends on its 4 parameters. For rotational freedom, θ_i is variable, and the other 3 parameters are fixed. For a revolute joint, the joint angle θ_i is the joint variable. According to the differential theory, the differentiation of Eq. (2) is:

$$\begin{aligned}\mathrm{d}\boldsymbol{A}_i &= \frac{\partial\boldsymbol{A}_i}{\partial a_i}\Delta a_i + \frac{\partial\boldsymbol{A}_i}{\partial\alpha_i}\Delta\alpha_i + \frac{\partial\boldsymbol{A}_i}{\partial d_i}\Delta d_i + \frac{\partial\boldsymbol{A}_i}{\partial\theta_i}\Delta\theta_i \\ &= \boldsymbol{A}_i\delta\boldsymbol{A}_i\end{aligned} \tag{3}$$

where Δa_i is the micro offset of a_i, $\Delta\alpha_i$ is the micro offset of α_i, Δd_i is the micro offset of d_i, $\Delta\theta_i$ is the micro offset of θ_i . $\delta\boldsymbol{A}_i$ is the error matrix of $\boldsymbol{A}_i$:

$$\delta\boldsymbol{A}_i = \begin{bmatrix} 0 & -\delta z_i^A & -\delta y_i^A & -\mathrm{d}x_i^A \\ \delta z_i^A & 0 & -\delta x_i^A & -\mathrm{d}y_i^A \\ \delta z_i^A & \delta x_i^A & 0 & -\mathrm{d}z_i^A \\ 0 & 0 & 0 & 0 \end{bmatrix} \tag{4}$$

in which $\mathrm{d}x_i^A$, $\mathrm{d}y_i^A$, $\mathrm{d}z_i^A$ are the position errors of frame $\{i\}$ with respect to frame $\{i-1\}$. δx_i^A, δy_i^A, δz_i^A are the orientation errors of frame $\{i\}$ with respect to frame $\{i-1\}$.

With consideration of the error, the transformation model between the robot coordinate system and the tool coordinate system is established:

$$\begin{aligned}\boldsymbol{T}_n + \mathrm{d}\boldsymbol{T}_n &= (\boldsymbol{A}_1 + \mathrm{d}\boldsymbol{A}_1)(\boldsymbol{A}_1 + \mathrm{d}\boldsymbol{A}_1)\ldots(\boldsymbol{A}_n + \mathrm{d}\boldsymbol{A}_n) \\ &= \prod_{i=1}^{n}(\boldsymbol{A}_i + \mathrm{d}\boldsymbol{A}_i)\end{aligned} \tag{5}$$

If we ignore the differential higher-order term, we can obtain:

$$\begin{aligned}\mathrm{d}\boldsymbol{T}_n &= \boldsymbol{T}_n\cdot\sum_{i=1}^{n}(\boldsymbol{U}_{i+1}^1\cdot\delta\boldsymbol{A}_i\cdot\boldsymbol{U}_{i+1}^1) \\ &= \boldsymbol{T}_n\cdot\delta\boldsymbol{T}_n\end{aligned} \tag{6}$$

where $\delta\boldsymbol{T}_n$ is the error matrix of $\boldsymbol{T}_n$, and $U_i^1 = A_1A_2\cdots A_n$. According to differential kinematics,

$$\begin{aligned}\delta\boldsymbol{T}_n &= \sum_{i=1}^{n}(\boldsymbol{U}_{i+1}^{-1}\cdot\delta\boldsymbol{A}_i\cdot\boldsymbol{U}_{i+1}) \\ &= \begin{bmatrix} 0 & -\delta z_n & \delta y_n & \mathrm{d}x_n \\ \delta z_n & 0 & -\delta x_n & \mathrm{d}y_n \\ -\delta y_n & \delta x_n & 0 & \mathrm{d}z_n \\ 0 & 0 & 0 & 0 \end{bmatrix}\end{aligned} \tag{7}$$

in which $\mathrm{d}x_n$, $\mathrm{d}y_n$, $\mathrm{d}z_n$ are the position errors of frame {n} with respect to frame {0}. δx_n, δy_n, δz_n are the orientation errors of frame $\{n\}$ with respect to frame {0}.

The position and orientation errors vectors of the end effector are expressed as:

$$\boldsymbol{d}_n = [\,\mathrm{d}x_n,\quad \mathrm{d}y_n,\quad \mathrm{d}z_n\,]^{\mathrm{T}} \tag{8}$$

$$\boldsymbol{\delta}_n = [\,\delta x_n,\quad \delta y_n,\quad \delta z_n\,]^{\mathrm{T}} \tag{9}$$

2.2. Robot position error similarity

Each component of the position error vector $\boldsymbol{d}^n$ is described by a series functions composed of the kinematic parameters:

$$\begin{cases}\mathrm{d}x_n = \mathrm{d}x(\theta_1,\theta_2,\ldots,\theta_n) \\ \mathrm{d}y_n = \mathrm{d}y(\theta_1,\theta_2,\ldots,\theta_n) \\ \mathrm{d}z_n = \mathrm{d}z(\theta_1,\theta_2,\ldots,\theta_n)\end{cases} \tag{10}$$

Each function is composed of algebraic functions and trigonometric functions. Therefore, there is a degree of similarity between the pose errors when the joints configurations are close. The similarity is related to the deviation of each joint angle between configurations. Robot inverse kinematic analysis has shown that the pose of a robot and its joint angles are connected by a functional relation. Therefore, the pose errors of a robot also exhibit similarity.

When a robot is in a specific pose, its position error $\boldsymbol{d}_n$ can be treated as a three-dimensional vector in the base coordinate system. The concept of error similarity has been proposed by

Zhou et al.[18] The error similarity for error vectors of any two poses is defined as:

$$\omega = \begin{cases} \infty & \boldsymbol{e}_1 = \boldsymbol{e}_2 \\ 1/|\boldsymbol{e}_1 - \boldsymbol{e}_2| & \boldsymbol{e}_1 \neq \boldsymbol{e}_2 \end{cases} \tag{11}$$

where $\boldsymbol{e}_1$ and $\boldsymbol{e}_2$ are the position vectors, and ω is the position error similarity.

2.3. Error compensation model based on error similarity

In this study, inverse weighted interpolation is used to calculate the position error. The method generates an evenly spaced grid according to a particular step in the workspace of a robot (see Fig. 1).

The grid vertex position errors are used to establish an error model for the grid through the inverse distance weight method (see Fig. 2). The error similarity between an arbitrary point P and the vertex $P_i (i = 1, 2, \ldots, 8)$ is negatively correlated to the distance. The correlated weight expression is as follows:

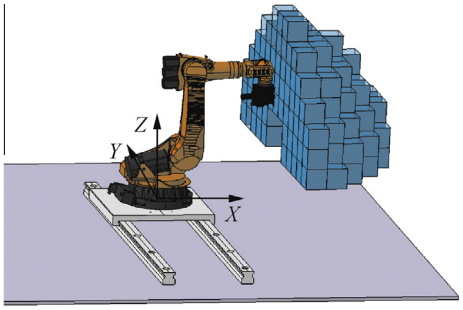

Fig. 1 Schematic of spatial grid generation.

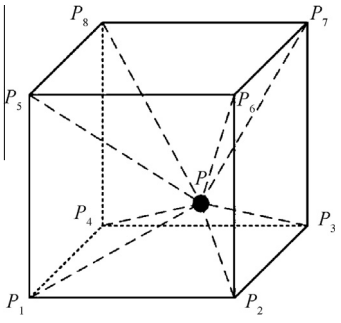

Fig. 2 Inverse-distance weight interpolation model.

$$q_i = \frac{(1/s_i)}{\sum_{j=1}^{8}(1/s_j)} \tag{12}$$

where q_i is the weight of point P relative to the vertex P_i, and s_i is the is the distance between point P and vertex point P_i.

The absolute position error vector for point P is predicted as:

$$\boldsymbol{e} = \sum_{i=1}^{8}(q_i \cdot \boldsymbol{e}_i) \tag{13}$$

where $\boldsymbol{e}$ is the position error vector prediction of point P, and $\boldsymbol{e}_i$ is the position error vector of the grid vertex P_i.

The error of the target position e is predicted. To complete the accuracy compensation, the coordinates of the target position in the control program must be corrected. The corrected coordinates are calculated as follows:

$$P' = P + \boldsymbol{e} \tag{14}$$

where P' is the theoretical position of point P after correction.

3. Analysis of the correlation between the error and the position

Depending on the method used for error compensation, sampling points will affect the compensation. On one hand, increasing the grid quantity increases the compensation accuracy. On the other hand, increasing the grid density also increases the workload for measurements. To analyze the position error distribution, an error identification model is used. A Kuka KR-210 robot is used as the test robot. A robot calibration method proposed by Zhong et al.[20] identified the 24 kinematics parameter errors. According to the method, the geometric parameter errors of the test robot are identified. In Table 1, Δa is the length error of the connecting rod, Δd is the offset error of the joint, $\Delta\alpha$ is the torsional angle error of the connecting rod, and $\Delta\theta$ is the torsional angle error of the joint.

Theoretically, the robot position error of any arbitrary point can be calculated using the kinematics parameter errors listed in Table 1. To view the correlation between the error and the position distance, an error range simulation of TCP (tool center point) is presented. There are 6 degrees of freedom at the end of the robot. However, to simplify the problem, only 2 of those degrees are allowed to move the positions in the X- and Y-directions. Table 2 lists the range of each degree of freedom, X is position range in X-direction, Y is position range in Y-direction, Z is position range in Z-direction, A is the angle range of rotation about Z-direction, B is the angle range of rotation about Y-direction, C the angle range of rotation about X-direction.

Table 1 Identified kinematic errors of a Kuka KR210 robot.

Link No.	Δa (mm)	Δd (mm)	$\Delta\alpha$ (rad)	$\Delta\theta$ (rad)
1	-0.32	-1.64	2.62×10^{-5}	-2.21×10^{-4}
2	-1.40	2.5×10^{-5}	2.44×10^{-5}	1.56×10^{-3}
3	0.78	3.59×10^{-5}	1.5×10^{-4}	-7.36×10^{-4}
4	-0.18	-0.29	-6.54×10^{-5}	1.05×10^{-4}
5	-2.89×10^{-2}	-2.5×10^{-6}	-6.2×10^{-4}	-6.14×10^{-4}
6	-3×10^{-5}	9×10^{-2}	5.58×10^{-4}	-6.1×10^{-6}

Table 2 Variation range of each degree of freedom.

Degree	X (mm)	Y (mm)	Z (mm)	A (°)	B (°)	C (°)
Arrange	1000–2000	−500–500	1800	0	90	0

Fig. 3(a)–(c) are the results of error range simulation. In which D_X represents the position error in X-direction, D_Y represents the position error in Y-direction, D_Z represents the position error in Z-direction.

The simulation results show that the change of the position error at the end of the robot is continuous with the change of position, which is in agreement with the pose error similarity described in Section 2.2. In addition, the error surface is also spatially variable. For different compensation spatial positions and sizes, the optimum error similarity planning methods for measurement of error compensation are also different.

4. Experimental for sampling point planning

There are 24 error parameters for the error model. It is complicated to process this model, and it is difficult to obtain the optimum planning of measurement through analysis. Therefore, a mathematical method based on statistics is used to determine the optimum measurement that would be widely suitable for use in the workspace of the robot. Because equal-interval cubic grid points are used, the optimum grid step is the primary parameter for the planning of sampling points.

4.1. Establishing the robot coordinate system

The robot coordinate system is located at the bottom of the robot. It is the reference coordinate system of the robot's mechanical structure. Because of the robot installation method and the restriction on the measuring range of the laser tracker (FARO SI), the robot coordinate system often cannot be directly measured in practice. The measurement software included in the laser tracker system can be used to establish the robot coordinate system by fitting as follows (see Fig. 4):

Step 1: The robot is maneuvered to the mechanical zero position.
Step 2: The base plane is determined. The base plane is located at the bottom of the robot. The SMR (spherically-mounted reflector) is placed on the installation plane of the robot through spatial scanning. As many points as possible are measured along the base of the robot for plane fitting. The base plane is obtained by offset of the fitted plane by the radius of the SMR.
Step 3: The origin and the Z-direction of the robot coordinate system are determined. The SMR is fixed on the flange at the end of the robot. The A_1 axis is rotated, and as many points as possible are measured to fit a circle, while keeping the positions (joint angles) of the A_2–A_6 axis stationary. The direction of the normal line of this circle is the Z-direction of the robot coordinate system. The intersection point between the normal line and the base plane is the origin of the robot coordinate system.
Step 4: The ZX-plane of the robot coordinate system is determined. When the robot is at the mechanical zero position, the SMR (∅38.1 mm) is placed on the 6 holes (∅10 mm) on the flange for measurement. The 6 points obtained from the measurement are used to fit a circle. The center of this circle is the point on the ZX-plane of the robot coordinate system (see Fig. 5).
Step 5: The robot coordinate system is established. The robot coordinate system is established through the origin of the coordinate system, the Z-direction, and the point on the ZX-plane.

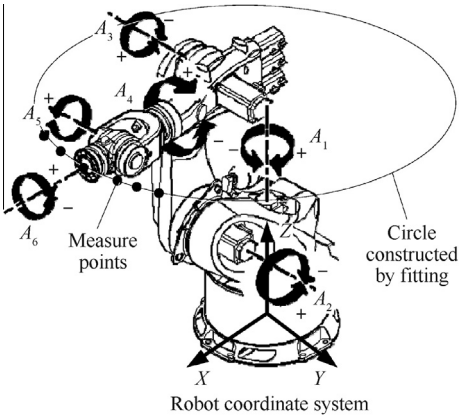

Fig. 4 Method to get the robot's A_1 axis using a laser tracker.

4.2. Experimental planning method

Analysis of the position errors in Section 2 shows that the error surface of the robot is spatially variable. It may lead the error

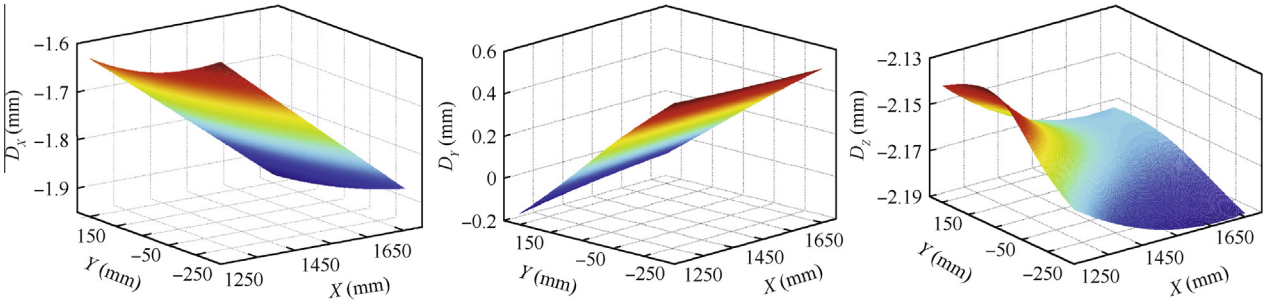

(a) D_X (b) D_Y (c) D_Z

Fig. 3 Error distributions of the robot TCP.

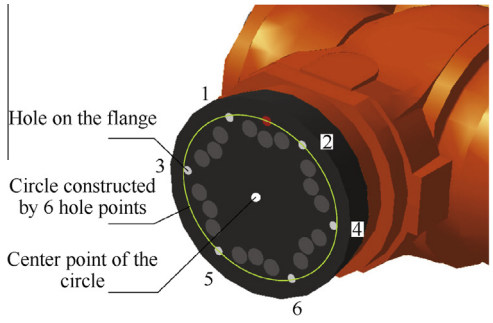

Fig. 5 Method to get the point on ZX-plane of the robot coordinate system.

compensations in different regions to respond differently to the same change in different grids. Therefore, several representative areas in the region to be calibrated are selected to analyze the variation of the compensation effect. Both a peripheral area and a central area in the given region are tested. In addition, the points close to the central points of the marginal area and the central area are used as the central points of the grids (see Fig. 6). To test the error compensation method of different grid sizes, several cubes with the same central point are chosen, and their side lengths increase with a fixed value. Then, the position errors of the grid vertex are obtained through measurement at the selected sampling points for error compensation. To examine the actual accuracy after compensation, the proposed error compensation method is used to correct the errors of the test points in the region. The measured position error is the actual compensation effect value when the grid side length is selected. The maximum and standard deviation of the position errors of different grid sizes after error compensation are mathematically analyzed to meet the accuracy requirement, and then the optimum grid size is selected (see Fig. 7).

Step 1: According to the error distribution in the region, experimental points within the given region are selected as grid central points.
Step 2: For each grid central point, the cubes are selected in different steps. The error similarity compensation method is used to correct the position error.
Step 3: For each selected grid step, statistics are conducted on the position accuracies of all the experimental points after compensation.
Step 4: The optimum grid step is selected. If a step had a relatively small standard deviation and a relatively long grid step and its absolute position error meets the accuracy requirements, then it is selected as the optimum grid step of the given region.

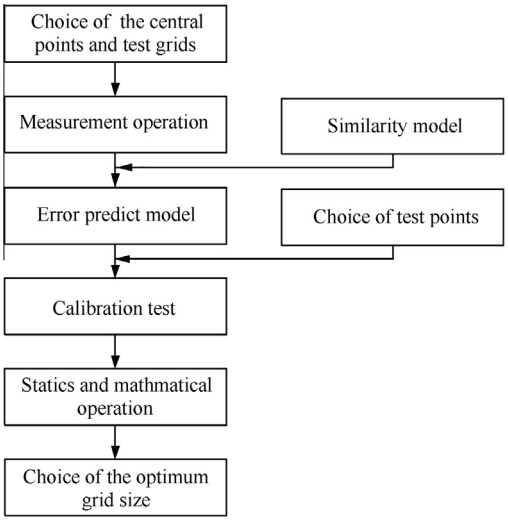

Fig. 7 Process of choosing the optimum grid size.

4.3. Selection method for experimental points

According to industrial robots performance criteria and related test methods up to China's national standard and professional standard (GB/T 12642—2001), 8 suitable positions must be determined within the cube of the working region to examine the pose accuracy of an industrial robot. As shown in Fig. 5, $C_i (i = 1, 2, \ldots, 8)$ are selected as the cubic vertices (see Fig. 8).

There are 4 planes to be selected for a pose experiment based on the standard requirement. In this case, the planes are C_1–C_2–C_7–C_8, C_2–C_3–C_8–C_5, C_3–C_4–C_5–C_6, and C_4–C_1–C_6–C_7. 5 points (P_1, P_2, P_3, P_4, and P_5) that must be measured are on the diagonals of the measuring planes in the standard requirement. P_1 is the center of the cube. The positions of other point P_2 to P_5 are shown in Fig. 9. To describe the errors within the entire grid space as much as possible, the points on the other two diagonals are added. 9 points $(P_1, P_2, \ldots, P_9)$ within each grid are selected as measurement points. In Fig. 9, L represents the length of the diagonal.

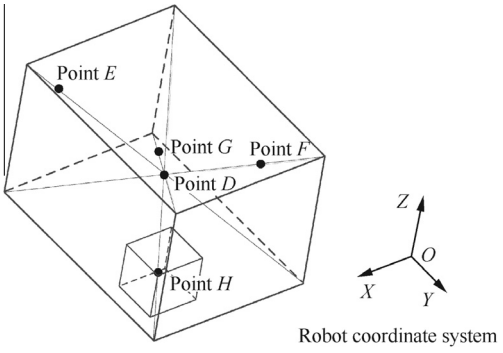

Fig. 6 Selection of choosing grid center points.

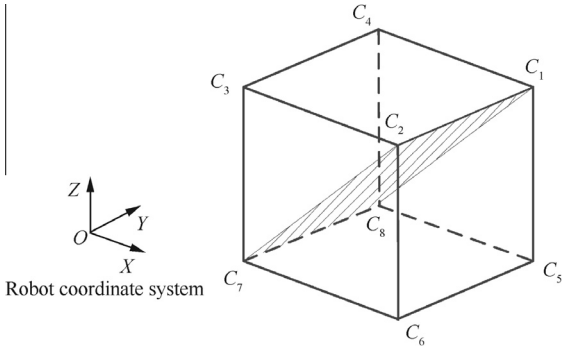

Fig. 8 Cubic vertices within the workspace.

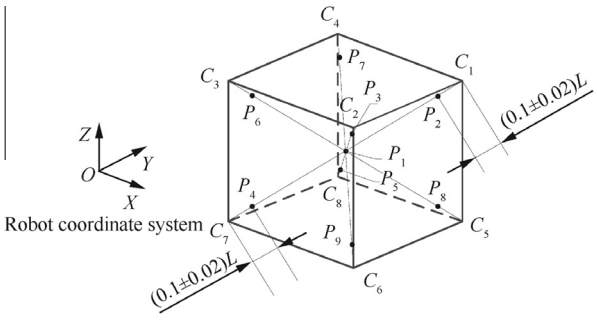

Fig. 9 Schematic for the selection of experimental points within a grid.

4.4. Statistical and mathematical method

When the cube is small enough to be close to a point, the predictive accuracy of the error model is close to the point's repeat accuracy. With increasing of the grid size, the predictive ability of the error model decreases. The maximum error and the standard deviation of the measurements are used as the criteria. The largest grid that meets the accuracy requirements is selected as the optimum compensation grid step in the region. The steps of the procedure are as follows:

Step 1: The maximum and minimum errors are determined based on the selected step. The standard deviations of all the error samples are also calculated based on the selected step.
Step 2: The maximum errors in different steps are combined with their corresponding steps to establish an error-step curve using the cubic polynomial interpolation method.
Step 3: The thresholds of the grid steps that meet the accuracy requirements are determined based on the error variation curve from Step 2.
Step 4: The optimum grid step is selected. If a step has a relatively small standard deviation and its maximum position error meets the accuracy requirements, it is selected as the optimum grid step of the given machining region.

5. Experimental

A KuKa KR210 industrial robot is used as the test robot. A Faro SI laser tracker is used to measure the optimum grid step in the experiment (see Fig. 10). During the experiment, the robot is under zero load and is operated in a working temperature environment of 15–18 °C. The target orientation and the operating speed of the robot are kept constant.

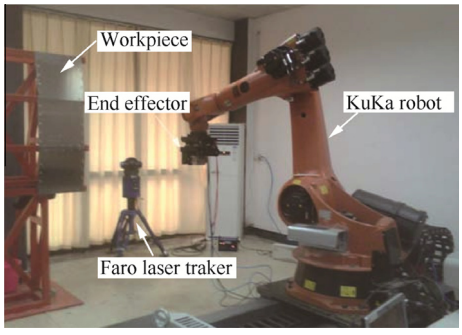

Fig. 10 Calibration setup.

The common working region of the robot is selected. The size of the region is 1000 mm × 1200 mm × 1000 mm (see Fig. 11). The accuracy requirement of TCP is preset as ±0.3 mm in each degree of freedom.

The analysis of the absolute position error of the robot in Section 2 shows that the error plane is spatially variable. The accuracy compensation effects in different areas in any selected region may be different. Therefore, based on the characteristics of the workspace, 5 grid central points are selected (see Table 3).

A growth step of 60 mm is selected. The grid's central point is selected as the start point and the step is gradually increased from 20 mm to 500 mm to establish 9 cubic grids. To reduce the effects of random errors during the measurements, 5 measurements are taken in each point to calculate the average value.

Table 4 shows the results of the test points' poison errors after calibration in different grid sizes. The statistical method described in Section 3.4 is applied to the experimental data.

To improve the effectiveness of the data, the mean maximum and minimum values of 5 measurements are used as the maximum and minimum values of the sample, respectively.

The maximum and minimum errors in the *X*-, *Y*-, and *Z*-directions are used to establish error-step distribution maps with cubic-polynomial interpolation, as shown in Fig. 12.

The analyses in Fig. 12 show that the errors in the *X*- and *Z*-directions increase as the grid step increases. The error compensation results in the *X*- and *Z*-directions decrease as the grid step increases. According to the error limit (±0.3 mm), the threshold of the step in the *X*-direction is in the range of 200–250 mm. For all grid steps tested in the *Y*-direction, up to and including 500 mm, the error is less

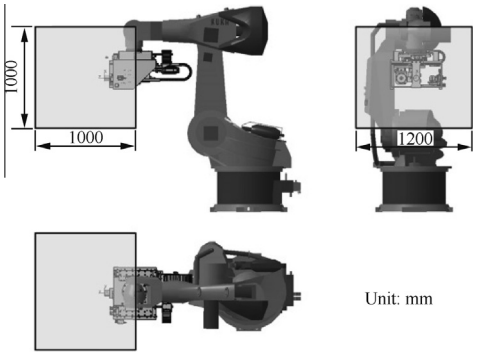

Fig. 11 Region for the error compensation experiment.

Table 3 Coordinate distribution of the measuring points.

Point	*X* (mm)	*Y* (mm)	*Z* (mm)	*A* (°)	*B* (°)	*C* (°)
D	1700	0	1500	0	90	0
E	2000	−350	1800	0	90	0
F	1400	350	1900	0	90	0
G	1400	−350	1400	0	90	0
H	2000	350	1400	0	90	0

Table 4 Position accuracy after error compensation in different steps.

Cube step (mm)	Measurement(mm)								
	Maximum			Minimum			Standard deviation		
	X	*Y*	*Z*	*X*	*Y*	*Z*	*X*	*Y*	*Z*
20	0.165	0.059	0.167	−0.016	−0.098	−0.06	0.05	0.04	0.073
80	0.182	0.211	0.21	−0.027	−0.266	−0.132	0.055	0.108	0.081
140	0.228	0.204	0.226	−0.074	−0.248	−0.176	0.064	0.105	0.109
200	0.279	0.213	0.265	−0.107	−0.224	−0.228	0.084	0.109	0.121
260	0.283	0.195	0.278	−0.119	−0.245	−0.262	0.102	0.108	0.13
320	0.393	0.183	0.461	−0.181	−0.261	−0.393	0.127	0.117	0.177
380	0.406	0.182	0.464	−0.189	−0.233	−0.372	0.13	0.112	0.198
440	0.493	0.205	0.556	−0.226	−0.235	−0.471	0.153	0.123	0.22
500	0.45	0.227	0.648	−0.271	−0.251	−0.443	0.16	0.122	0.238

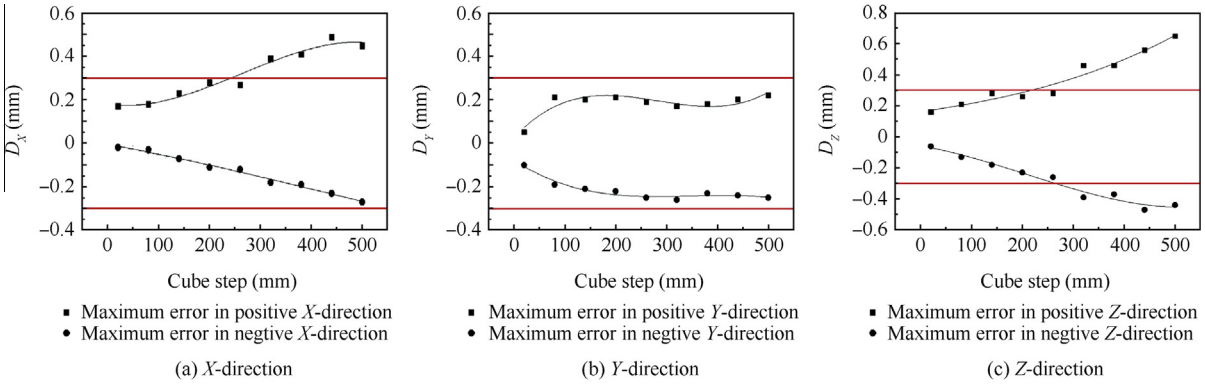

Fig. 12 Position error curves of the robot TCP after compensation from 20 mm to 500 mm.

Table 5 Verification test results of optimal samples.

Calibration	Measurement(mm)								
	Max			Minimum			Standard deviation		
	X	*Y*	*Z*	*X*	*Y*	*Z*	*X*	*Y*	*Z*
Before	0.598	0.272	0.045	−0.282	−0.675	−1.068	0.193	0.150	0.252
After	0.167	0.270	0.240	−0.144	−0.217	−0.216	0.061	0.101	0.084

than ±0.3 mm. The threshold of the step in the *Z*-direction is in the range of 200–250 mm. The variation of the standard deviation of the errors is relatively small in the range of 140–260 mm. Considering the statistical results and the convenience of the region partition, 200 mm is selected as the optimum grid step.

Following the above analysis, a 200-mm grid step is selected to generate the grid for error compensation for the KuKa KR210 robot. The error compensation algorithm is used to measure the position errors of 200 random points in the workspace after error compensation. The experimental results (see Table 5) show that the maximum/minimum values of the unidirectional position errors of the 200 points are 0.27/−0.22 mm, respectively. Therefore, this planning method for sampling configurations effectively reduces the difficulty in finding error compensation sampling configurations. The experimental results show that the position accuracy of the robot can be increased to the required accuracy using this method.

6. Conclusions

(1) Based on the characteristics of the position errors of robots, an error compensation model based on error similarity is established. A simulation is performed to analyze the distribution of the position errors of a Kuka KR210 robot. It is discovered that the variation of the position errors of the robot is continuous and the error surface is spatially variable. The selected measurement for error compensation is different in different regions of sizes and positions in Cartesian space.

(2) A method for choosing robot error compensation sampling configurations is proposed based on statistical analysis. 5 topical areas in Cartesian space are selected to test the error compensation method based on the model of error similarity. The result of the test is used to choose the optimal grid step based on a statistical analysis. A test of the method is used on the Kuka KR210 robot. The optimal grid step is 200 mm.

(3) An experimental setup with the robot and a laser tracker is constructed. The proposed mathematical planning method for robot error compensation sampling configurations is verified. According to the experimental results, the optimal grid step that meets the accuracy requirement can be selected by statistical analysis. The number of measurement configurations is effectively reduced.

Acknowledgements

This study was co-supported by the National Natural Science Foundation of China (No. 51475225) and the Aeronautical Science Foundation of China (No. 2013ZE52067).

References

1. Bi SS, Liang J. Robotic drilling system for titanium structures. *Int J Adv Manuf Technol* 2011;**54**(5–8):767–74.
2. Devlieg R, Sitton K, Feikert E, Inman J. ONCE (one-sided cell end effector) robotic drilling system. SAE International; 2002 Oct 1–3. Report No.: 2012–01-2626.
3. Atkinson J, Hartmann J, Jones S, Gleeson P. Robotic drilling system for 737 aileron. SAE International; 2007 Sep 17–20; Report No.: 2007–01-3821.
4. Bogue R. Europe fights back with advanced manufacturing and assembly technologies. *Assem Autom* 2012;**32**(4):312–7.
5. Zhou F. Robotic era for aircraft assembly. *Aeronaut Manuf Technology* 2009(24);34–7 Chinese.
6. Roth ZS, Mooring B, Ravani B. An overview of robot calibration. *IEEE J Robot Automat* 1987;**3**(5):377–85.
7. Stone HW, Sanderson AC. Statistical performance evaluation of the S-model arm signature identification technique*Proceedings of 1988 IEEE international conference on robotics and automation; 1988 Apr 24–29; Philadelphia, PA*. New York: IEEE; 1988. p. 939–46.
8. Denavit J, Harterberg RS. A kinematic notation for lower-pair mechanisms based on matrices. *Trans ASME J Appl Mech* 1955;**22**:215–21.
9. Zhuang HQ, Roth ZS, Hamano F. A complete and parametrically continuous kinematic model for robot manipulators. *IEEE Trans Robot Automat* 1992;**8**(4):451–63.
10. Veitschegger WK, Wu CH. Robot calibration and compensation. *IEEE J Robot Automat* 1988;**4**(6):643–56.
11. Wang W, Wang G, Yun C. A calibration method of kinematic parameters for serial industrial robots. *Industr Robot Int J* 2014;**41**(2):157–65.
12. Nubiola A, Bonev IA. Absolute calibration of an ABB IRB 1600 robot using a laser tracker. *Robot Comput-Integr Manuf* 2013;**29**(1):236–45.
13. Motta JMST, de Carvalho GC, McMaster RS. Robot calibration using a 3D vision-based measurement system with a single camera. *Robot Comput-Integr Manuf* 2001;**17**(6):487–97.
14. Ginani LS, Motta JMST. Theoretical and practical aspects of robot calibration with experimental verification. *J Braz Soc Mech Sci Eng* 2011;**33**(1):15–21.
15. Wang DL, Bai Y. Improving position accuracy of robot manipulators using neural networks*Proceedings of the IEEE instrumentation and measurement technology conference; 2005 May 16–19; Ottawa, Canada*. New York: IEEE; 2005. p. 1524–6.
16. Park IW, Lee BJ, Cho SH, Hong YD, Kim JH. Laser-based kinematic calibration of robot manipulator using differential kinematics. *IEEE/ASME Trans Mechatron* 2012;**17**(6):1059–67.
17. Sun Y, Hollerbach JM. Observability index selection for robot calibration*2008 IEEE international conference on robotics and automation; 2008 May 19-23; Pasadena, CA, USA*. New York: IEEE; 2008. p. 831–6.
18. Zhou W, Liao WH, Tian W. Theory and experiment of industrial robot accuracy compensation method based on spatial interpolation. *Chin J Mech Eng* 2013;**49**(3):42–8.
19. Tian W, Zeng YF, Zhou W, Liao WH. Calibration of robotic drilling systems with a moving rail. *Chin J Aeronaut* 2014;**27**(6):1598–604.
20. Zhong XL, Lewis J, N-Nagy FL. Inverse robot calibration using artificial neural networks. *Eng Appl Artif Intell* 1996;**9**(1):83–93.

Tian Wei received his B.S., M.S., and Ph.D. degrees from Nanjing University of Science and Technology in 2000, 2003, and 2006, respectively, and then became an instructor at Nanjing University of Aeronautics and Astronautics. Now he is an Associate Professor. His main research interests are digital flexible assembly, green remanufacturing, and so on.

Mei Dongqi received his B.S. degree from Nanjing University of Aeronautics and Astronautics in 2012, where he is now a master's degree candidate. His research field is robot calibration for aircraft flexible assembly systems.